2021 NDIA GROUND VEHICLE SYSTEMS ENGINEERING AND TECHNOLOGY SYMPOSIUM
MODELING SIMULATION & SOFTWARE TECHNICAL SESSION
AUGUST 10-12, 2021 - NOVI, MICHIGAN

A HYBRID REDUCED ORDER MODELING APPROACH FOR RAPID TRANSIENT THERMAL SIMULATION AND SIGNATURE ANALYSIS

Yi Wang[1*], William C. Krolick[2], Andrew L. Kaminsky[2], Nathan Tison[3], Yeefeng Ruan[3], Vamshi Korivi[3], Kapil Pant[2]

[1]Mechanical Engineering, University of South Carolina, Columbia, SC
[2]CFD Research Corporation, Huntsville, AL
[3]US Army DEVCOM Ground Vehicle Systems Center, Warren, MI

ABSTRACT

This paper presents a hybrid CFD and reduced order modeling (ROM) approach for fast and accurate flow and thermal analysis of vehicles to enable rapid thermal signature prediction. The modular hybrid ROM solver includes several key components, such as the turbulence modeling, CFD full order model (FOM) customized for vehicle thermal analysis, FOM/ROM alternation, proper orthogonal decomposition (POD) for basis vector construction, and online model switch decision maker for coupled simulation, which are all developed in an integrated framework. Several case studies of Army relevance at increasing complexity levels are undertaken. The proposed hybrid ROM solver is able to accurately analyze flow, turbulence, and thermal phenomena under time-varying operating conditions with unprecedented computational performance. Quantitatively, the relative error of our hybrid CFD FOM/ROM simulation stays below 0.35% and the absolute error is less than 4 K. The ROM has a much smaller model order (typically 10-15) relative to the CFD FOM. Speedup ratio up to 27× is achieved in the present study without the use of any hardware accelerate technique.

Citation: Y. Wang, W.C. Krolick, A.L. Kaminsky, N. Tison, Y. Ruan, V. Korivi, K. Pant, "A Hybrid Reduced Order Modeling Approach for Rapid Transient Thermal Simulation And Signature Analysis", In *Proceedings of the Ground Vehicle Systems Engineering and Technology Symposium* (GVSETS), NDIA, Novi, MI, Aug. 10-12, 2021.

1. INTRODUCTION

The survivability of military vehicles and their occupants often depends on efficient control of the vehicle's thermal infrared (IR) signature. IR emissions, stemming from the thermal load of military vehicles are used to detect, track, and lock-on to the target. Thermal and flow modeling is typically used to achieve performance goals related to the control of IR signatures. A key part of the thermal analysis of ground vehicles is the prediction of the thermal fields and convection heat transfer (CHT). Thermal modeling tools capable of accurately analyzing the thermal characteristics at multiple conditions for rapid design and reliable

*Corresponding Author: Associate Professor, University of South Carolina, yiwang@cec.sc.edu

thermal management are of paramount importance to DoD for enhancing thermal signature control, military vehicle survivability, situational awareness, and mission effectiveness.

Most existing thermal and flow modeling and simulation (M&S) capable of analyzing vehicle thermal signature is based on CFD. However, the prohibitive computational costs (e.g., runtimes of hours or longer depending on the model size and computational platform) and the need for a significant level of expertise and participation from the users for model setup [1] render them ill-suited for multi-condition parametric design analysis or applications where the fast simulation speed is needed. Consequently, the trade space to evaluate vehicle system performance cannot be thoroughly explored.

These limitations along with strong demands for rapid transient thermal and flow modeling and thermal signature analysis for military ground vehicles call for a modeling method and software that can capture critical thermal and flow behavior and enable rapid and accurate prediction of thermal field. It would also be desirable to allow the end-user to control, by setting the value of a solver input parameter, the balance between prediction accuracy and simulation time. In this context, various nonlinear reduced order modeling (ROM) and machine learning techniques have been explored, which however require time-consuming training simulations for model generation [1, 2]. This paper presents the development of a hybrid ROM approach for rapid and accurate prediction of thermal fields of ground vehicles at various simulation conditions. Our hybrid ROM methodology is based on adaptive alternation of the simulation between the full order model (FOM) and the ROM along the temporal trajectory [3, 4]. Because of the fast speed of the ROM, the computation of the hybrid model achieves salient computational efficiency. Meanwhile the modeling and simulation accuracy is also maintained.

2. METHODOLOGY

As shown in Figure 1, the whole simulation is divided into several intervals in the time domain. The span of each interval is denoted as Δt, which will be simulated by either FOM or ROM with a different time step δt that is much smaller than Δt.

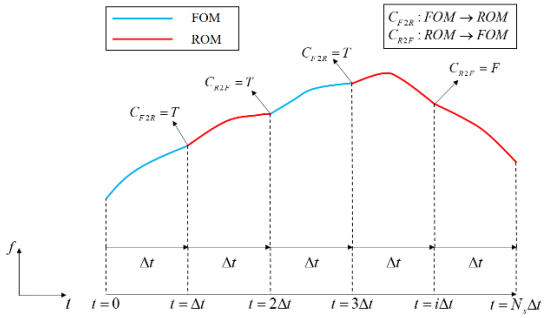

Figure 1. Schematic of the hybrid FOM/ROM computation methodology

Figure 1 also shows that the FOM for the conjugate heat transfer analysis involving both the flow and thermal solution will be used in the first time interval Δt. At the end of the interval, the proper orthogonal decomposition (POD) modes $\mathbf{U}_q$ will be computed using the singular value decomposition (SVD), and a criterion (C_{F2R}, see Section 2.3) will be evaluated to decide if the solution method should be switched from FOM to ROM in the next interval, i.e., $\Delta t \rightarrow 2\Delta t$. Correspondingly, there are two possibilities for the 2nd interval:

(1) If C_{F2R} is not satisfied, the FOM remains in use during $\Delta t \rightarrow 2\Delta t$, which generates more FOM data carrying new subspace information not present in previous POD modes. Therefore, the prior projection matrix $\mathbf{U}_q$ will be recomputed or updated by incorporating the new FOM solutions at the end, i.e., at $2\Delta t$. To reduce the computational cost associated with SVD, the POD modes $\mathbf{U}_q$ are updated using the incremental SVD (iSVD).

(2) On the other hand, if C_{F2R} is satisfied, the ROM use only involves the heat transfer solution by freezing the flow field obtained from the last solution in FOM during the interval $\Delta t \rightarrow 2\Delta t$.

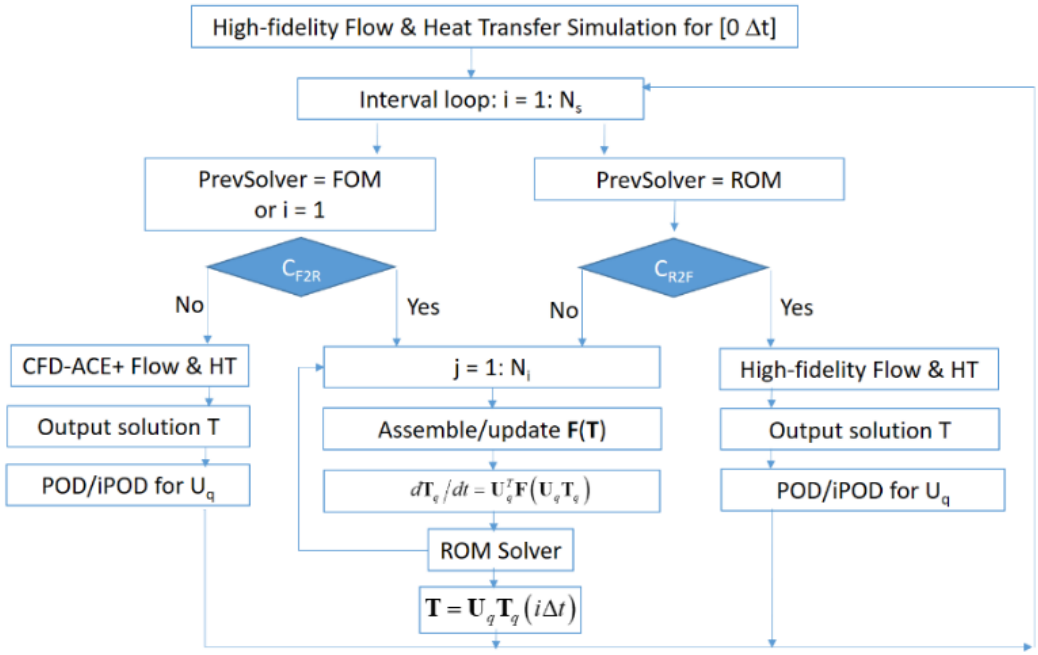

Figure 2. Detailed procedure to perform hybrid FOM/ROM computation. Four possibilities exist for model switching.

The FOM is projected onto the subspace spanned by $\mathbf{U}_q$ above to construct the ROM for use in the interval of $\Delta t \rightarrow 2\Delta t$. iSVD is not performed because the ROM trajectory lies within the prior subspace, and contributes no new data to the snapshot. In other words, the ROM is used in the temporal interval where there is little new subspace information to rapidly bridge the FOM simulation for reduced simulation cost. At the end of this interval, i.e., at $t = 2\Delta t$, another criterion C_{R2F} is examined to decide which model, FOM or ROM is used in the next interval, i.e., $2\Delta t \rightarrow 3\Delta t$. If true, the computation switches back to FOM. Otherwise, ROM remains in use.

The process above continues until all the intervals are simulated. This approach markedly accelerates the process of snapshot data and ROM generation, because there is a significant amount of redundant information in the FOM-based simulation as indicated by the high ratio of POD mode truncation in most cases. Figure 2 illustrates the detailed procedure of the hybrid simulation, which includes four possibilities of involving FOM or ROM simulation depending on the solver used in the previous interval, and the criteria of model switch (see Section 2.3).

2.1. Turbulence Modeling

The turbulent flow is simulated by CFD full order model (FOM), and then the convection terms and the turbulent thermal conductivity at the faces between computational cells and the solid-fluid wall are used for simulation of the heat transfer. In this work, the k-ε turbulence model is included in our FOM simulation. The effective thermal conductivity (consisting of both the laminar and the turbulent conductivity) is considered, and takes into account the turbulence effects on heat transfer. The effective thermal conductivity is given by

$$k_{eff} = k + \mu_t C_p / \sigma_t \quad (1)$$

where k is the laminar thermal conductivity; μ_t is the turbulent viscosity; C_p is the specific heat; σ_t is an empirical value ranging from about 1.0 near walls to 0.7 or less as it moves away from the wall. The default value of 0.9 is used herein. Note that the k-ε model is a high Reynolds number model and

is ill-suited for use in the near-wall regions where the viscosity effects are more dominant. Therefore, wall functions are used in the cells next to the walls.

2.2. Heat Transfer Modeling

In this work, the equations for the conjugate heat transfer analysis and the procedure to obtain the full-order thermal models and construct ROM are established. The flow only occurs in the fluid domains external and internal to the vehicle while the heat transfer takes place across all the domains including both the fluid and the solid domains. Both are linked via two-way coupling, viz., the flow contributes to the convective heat transfer; and the temperature affects the fluid viscosity and flow velocity. Thus, the governing equation of heat transfer in the entire domains can be written as

$$\rho C_p \,\partial T/\partial t = \nabla\cdot\left(k_{eff}\nabla T\right) - \rho C_p \mathbf{v}\cdot\nabla T + Q \qquad (2)$$

where $\mathbf{v}$ is the velocity vector of fluid flow; T is the temperature in the entire domain; ρ, k, and C_p are, respectively, the density, thermal conductivity, and specific heat of the materials; and Q is the heat source or sink terms. Our focus is mainly on the acceleration of the transient heat transfer with the assumption that the background flow is pre-calculated. This is a relatively good assumption as the temperature effects on the viscosity (and hence on flow velocity) are significantly weaker than those of the convection on heat transfer. Accordingly, during the thermal simulation (in the hybrid simulation), the flow fields, the fluid viscosity and flow velocity are pre-calculated and "frozen". This captures the dominant, first-order convective effect on the heat transfer.

The spatial differentials (i.e., R.H.S.) of the thermal governing equation (2) can be discretized by means of various numerical schemes, including the finite volume method (FVM), the finite difference method (FDM), or the finite element method (FEM). Since the FVM discretization is one of the most widely used methods in CFD, our hybrid FOM/ROM simulation is developed for the FVM, yielding

$$\begin{aligned}\rho C_p V_{\mathrm{P}}\frac{\partial T_{\mathrm{P}}}{\partial t} &= -\left(F_e+F_s+D_e+D_s+D_w+D_n\right)T_{\mathrm{P}} + \\ &\left(F_w+D_w\right)T_{\mathrm{W}}+\left(F_n+D_n\right)T_{\mathrm{N}}+D_eT_{\mathrm{E}}+D_sT_{\mathrm{S}}+Q_{\mathrm{P}}V_{\mathrm{P}} \\ &= -\left(F_w+F_n+D_e+D_s+D_w+D_n\right)T_{\mathrm{P}}+\left(F_w+D_w\right)T_{\mathrm{W}}+ \\ &\left(F_n+D_n\right)T_{\mathrm{N}}+D_eT_{\mathrm{E}}+D_sT_{\mathrm{S}}+Q_{\mathrm{P}}V_{\mathrm{P}} \\ &= -a_pT_{\mathrm{P}}+a_wT_{\mathrm{W}}+a_nT_{\mathrm{N}}+a_eT_{\mathrm{E}}+a_sT_{\mathrm{S}}+Q_{\mathrm{P}}V_{\mathrm{P}}\end{aligned} \qquad (3)$$

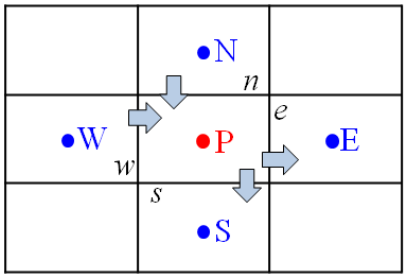

Figure 3. FVM representation of full-scale thermal model in a 2D computational domain

where P is the present cell of interest; E, S, W, and N are the center of the cells surrounding cell P; and e, s, w, n in the subscript are the interfaces linking the cell P with its adjacent cells (see Figure 3). T_{P} is the temperature at the cell center; V_{P} is the volume of the cell P; $F_i = (\rho v C_{\mathrm{P}} A)_i$ is convective links at the cell interface, A is the area of the interface, and subscript i is the index of the interface "e", "s", "w" and "n". $D_i = (kA/\delta)_i$ are the conductive links at the cell interface, where δ is the distance between the cell P and its neighboring cell. $Q_{\mathrm{P}}V_{\mathrm{P}}$ is the heat generation in the present cell, t is the time. $a_e = D_e$, $a_s = D_s$, $a_w = F_w+D_w$, $a_n = F_n+D_n$, and $a_{\mathrm{P}} = a_e+ a_s+a_w+a_n$. Within the solid domain, the convection terms (F_i) vanish. Eq. (3) is applied to all the computational cells in the domain including those at the boundaries, yielding a large system of ODEs governing the temperature evolution at each cell center. Subsequently the temporal term in Eq. (3) can be discretized by the Crank-Nicolson method, yielding,

$$\mathbf{M}_n^{m-1}\left(\mathbf{T}_n^m-\mathbf{T}_{n-1}\right)\Big/\Delta t = \left(\tilde{\mathbf{A}}_n^{m-1}+\mathbf{S}_p^{n,m-1}\right)\left[\alpha\mathbf{T}_n^m+(1-\alpha)\mathbf{T}_{n-1}\right]+\mathbf{S}_u^{n,m-1} \qquad (4)$$

where $\mathbf{T}(t)\in\Re^M$ is a vector storing the temperature at all the computational cells (in FVM formulation), and M is the total number of computational cells in the domain. $\mathbf{S}_p$ is the linear coefficient of the source term arising from the boundary or volumetric

conditions; and $\mathbf{S}_u$ is the constant source term inside the vehicle model. $\tilde{\mathbf{A}} \in \Re^{N\times N}$ is the thermal exchange matrix containing all the conductive and convective links described in Eq. (3); and $\mathbf{M}$ is the matrix storing the thermal mass of each cell. Subscript/superscript n and n-1 denote the quantities at the current and the previous time step, respectively, and superscript m denotes the m^{th} iteration in the n^{th} time step; and α determines the contribution of temperature from the current and the previous time steps when computing spatial terms. α = 1 or 0, respectively, reduces Eq. (4) to the fully implicit or explicit form. Eq. (4) then can be written as a shorthand notation

$$\mathbf{A}_n^{m-1}\mathbf{T}_n^m = \mathbf{b}_n^{m-1} \quad \text{or} \quad \mathbf{AT} = \mathbf{b} \tag{5}$$

It can be computed using a well-established direct solver or iterative solver, e.g., Generalized minimal residual method, conjugate gradient method, etc.

2.3. FOM-ROM Switch Criteria

In this work, the online decision-making capability to switch between the FOM and ROM during the simulation is also implemented. It compares the singular values of the POD modes and the trajectory of the temperature in the reduced domain with respect to several criteria at the end of each interval in order to maximize the computing efficiency. The algorithm is illustrated in Figure 4. The details are elucidated below:

1. Switching from FOM to ROM (Figure 4a): It is based on the distribution of the singular values σ_i as each σ_i determines the significance of the corresponding POD basis vector/mode to the subspaces of the snapshot solution. The first criterion $C_{\text{F2R,1}}$ is defined as the cumulative energy ratio of the truncated modes, i.e., mode number from n+1 to N. n will be selected in such a way that $C_{\text{F2R,1}}$ is smaller than a prescribed tolerance ε_1 to ensure the resulting ROM is numerically accurate to approximate the FOM from the energy perspective

$$C_{F2R,1} = \sqrt{\sum_{j=n+1}^{N}\sigma_j^2 \Big/ \sum_{i=1}^{N}\sigma_i^2} \le \varepsilon_1 \quad \text{and} \quad C_{F2R,2} = \sqrt{\sum_{j=n_1+1}^{N}\sigma_j^2 \Big/ \sum_{i=1}^{N}\sigma_i^2} \le \varepsilon_2 \tag{6}$$

   The first criterion, $C_{F2R,1}$ in Eq. (6) only quantitates the cumulative energy in the POD modes up to n, and is not able to monitor the variation in energy beyond n. Thus, the second criterion $C_{F2R,2}$ is defined to quantitatively evaluate the cumulative energy contained within the POD modes from n_1+1 to N. n_1 will also be selected to ensure the criterion is satisfied with respect to a smaller prescribed tolerance ε_2. n_1 is the number of the POD modes retained and will be the true order of the ROM.
2. Switch from ROM back to FOM (Figure 4b): A criterion is evaluated at the end of the ROM interval to determine which model should be employed in the next interval

$$C_{R2F} = \sqrt{\sum_{j=n+1}^{n_1+1}\left(\mathbf{T}_q^j\right)^2 \Big/ \sum_{j=1}^{N}\left(\mathbf{T}_q^j\right)^2} \ge \varepsilon_3 \tag{7}$$

where $\mathbf{T}_q$ represents the ROM solution at the end of the interval. Eq. (7) utilizes the energy associated with the extended POD modes bases (n-n_1) as a probe to examine if it is appropriate to continue using the ROM for the next interval. When the magnitude of $\mathbf{T}_q$ in the n_1-n extended basis grows significantly and exceeds the tolerance ε_3, it implies that the ROM is no longer able to follow the manifold of the system, and the simulation will switch back to FOM.

Note that due to their different dimensions, the FOM solution at the last time step in the interval needs to be projected onto the updated POD modes when the solver starts to change from FOM to ROM. On the other hand, the solution at the end of the ROM interval returns to the full domain, when the solver switches from ROM back to FOM. In this manner, the FOM and ROM solver can be stitched seamlessly during the whole simulation process.

2.4. Proper Orthogonal Decomposition

Since the dimension m of Eq. (5) is normally very high entailing demanding computation, the ROM technique is used to reduce the dimension from m to a much lower value of n_1 by projecting the original FOM onto a low-dimensional subspace

$\mathbf{U}_q \in \Re^{m \times n1}$ (i.e., $\mathbf{T} = \mathbf{U}_q \mathbf{T}_q$) constructed by a set of orthonormal basis vectors, where $\mathbf{T}_q \in \Re^{n1}$ is the temperature in the reduced domain and $n_1 << m$. In the present research, a mathematically rigorous ROM algorithm, i.e., proper orthogonal decomposition (POD) is used to identify $\mathbf{U}_q$ and automatically generate thermal ROMs amenable to fast computation by direct solvers. POD [5] is a powerful method for data reduction and ROM [6, 7], and is well-suited for efficient modeling and analysis of the vehicle heat transfer. To implement POD, the method of snapshots is used, which extracts the leading POD modes using an ensemble of data (snapshots) from the FOM computation [8]. In our hybrid FOM/ROM simulation, the snapshot data is obtained from the FOM simulation prior to the ROM simulation. Given a matrix $\mathbf{\Gamma}$ containing the temperature snapshots at certain instants of time t_l in FOM simulation

$$\mathbf{\Gamma} = \left[\mathbf{T}(t_1)\,\mathbf{T}(t_2)\cdots\mathbf{T}(t_l)\cdots\mathbf{T}(t_N)\right] \tag{8}$$

where $\mathbf{T}(t_l)$ is the l^{th} snapshot in time; $l = 1, 2, \ldots, N$ and N is the total number of the snapshots and also the number of time steps within an interval. $\mathbf{\Gamma}$ can then be factorized using the singular value decomposition (SVD), followed by truncation at the first $n_1 << m$ leading modes yielding

$$\mathbf{\Gamma} = \mathbf{U}\Sigma\mathbf{V}^T \approx \mathbf{U}_q \Sigma_q \mathbf{V}_q^T,\ \mathbf{U}_q \in \Re^{m \times n_1},\ n_1 << m \tag{9}$$

where $\mathbf{U}_q \in \Re^{m \times n1}$ is the dominant subspace comprised of n_1 leading POD modes spanning the original snapshot matrix, $\mathbf{\Sigma}_q \in \Re^{n1 \times n1} = \text{diag}(\sigma_i)$ is a diagonal matrix of singular values arranged in a descending order. The singular value σ_i measures the dominance of its associated column in $\mathbf{U}_q$. Therefore, by examining the relative magnitude of σ_i, an appropriate number n_1 can be determined for ROM that yields desired model accuracy; and $\mathbf{V} \in \Re^{N \times n1}$ is the mode in the temporal domain. The original FOM in Eq. (5) then can be projected onto the subspace $\mathbf{U}_q$ yielding a ROM with a much lower dimension (i.e., $n_1 << m$):

$$\mathbf{A}_q \mathbf{T}_q = \mathbf{b}_q \tag{10}$$

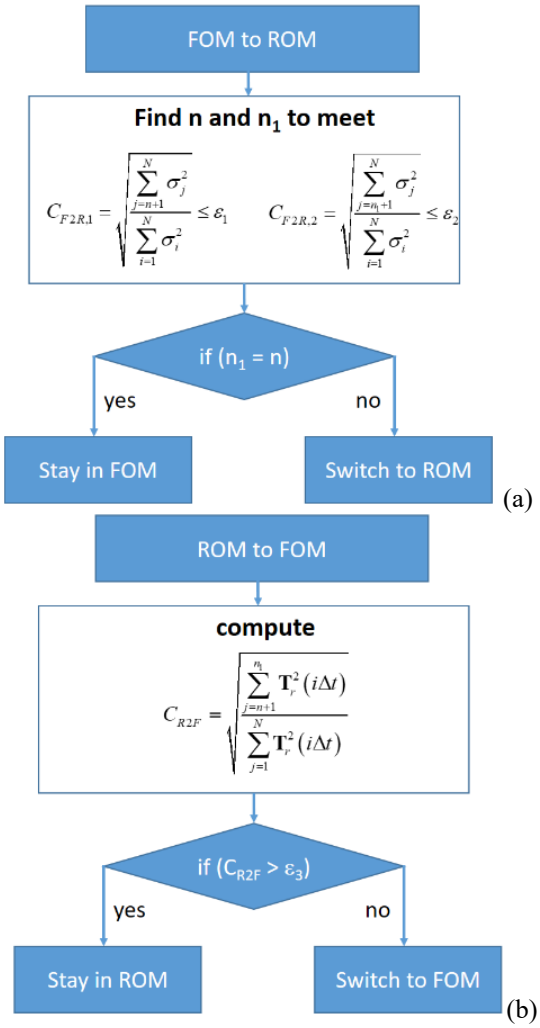

Figure 4. Automated switch between FOM and ROM during online simulation

where $\mathbf{A}_q = \mathbf{U}_q{}^T\mathbf{A}\mathbf{U}_q$ and $\mathbf{b}_q = \mathbf{U}_q{}^T\mathbf{b}$. Given its significantly lower dimension, the ROM governing $\mathbf{T}_q$ can be computed at much faster speed relative to the FOM. A critical limitation of the POD is the demanding requirement of physical memory to accommodate massive CFD data sets and low computational efficiency when new snapshot data becomes available for processing. In the present work, an incremental SVD (iSVD) technique, which treats the entire dataset as an ensemble of data packets and processes the data packet one by one. Such a "divide and conquer" strategy significantly reduces computational time and resource requirements by making use of a

continuous, incremental updating of the POD modes that manipulates markedly smaller data subsets and enables salient scalability of the algorithm. The iSVD implementation [3, 4, 9] includes four key steps, i.e., projecting the new data onto the previous subspace, calculating the error residual due to projection, computing the correction terms, and rotating and updating the POD modes and coefficient matrix. In our framework, iPOD is performed following the FOM simulation. Once the new POD modes become available, they are either used for the ROM simulation or further updated by additional FOM data in the next interval.

3. RESULTS AND DISCUSSION

The key technological components, including the high-fidelity CFD, hybrid simulation (FOM/ROM alternation), online model switch, and POD and iPOD are verified with relevant case studies. Simplified 2D and 3D vehicle models with different operating scenarios are analyzed.

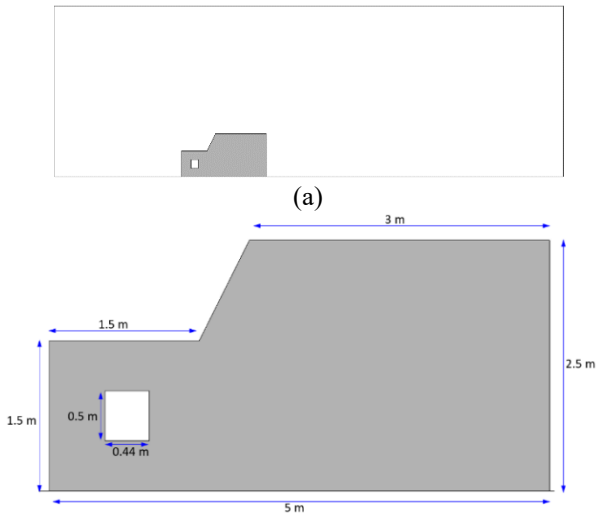

Figure 5. Computational domain and the simplified 2D vehicle model: (a) entire domain; and (b) vehicle

3.1. 2D Simplified Vehicle

The case studies and technology validation are first carried out for a 2D simplified vehicle model. Figure 5a shows the computational domain, which contains two subdomains: the solid vehicle (in gray) and the fluid flow domain (in white within the bounding box). The dimensions of the simplified vehicle are shown in Figure 5b. The rectangular region of 0.5 m×0.4 m within the vehicle represents the engine box. The computational domains are meshed using the structured grids, yielding 19,375 computational cells.

The computed turbulent thermal conductivity is typically much higher than the laminar conductivity and location-dependent (see Figure 6), and represents the greatest contribution to heat transfer in the airflow domain. In addition, an inlet flow velocity of 10 m/s is specified at the left boundary of air domain. The top and the right boundaries are given the outlet boundary condition. The bottom of the domain is treated as an adiabatic wall.

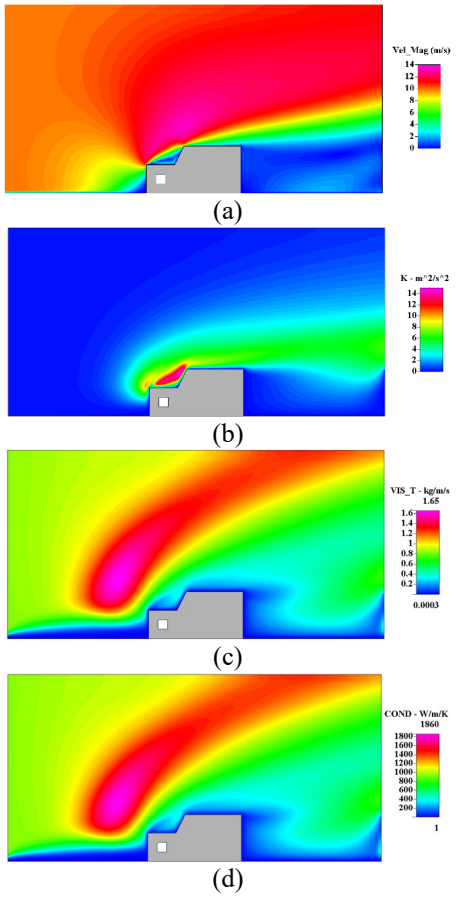

Figure 6. Spatial distribution of the flow and turbulence quantities: (a) velocity magnitude; (b) kinetic energy; (c) turbulent viscosity; and (d) effective conductivity.

Figure 7 illustrates the POD modes of the temperature field. The first several modes exhibit dominant thermal structures and the first one virtually represents the mean temperature field. Higher-order modes feature a larger number of thermal structures with shorter length scales, and hence, representing local modification of the temperature field with less contribution.

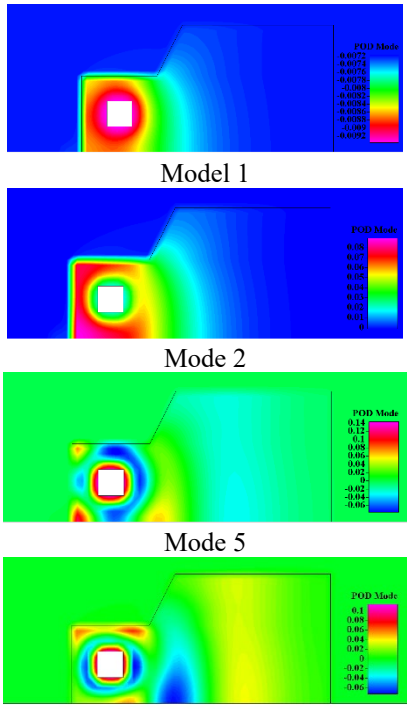

Figure 7. POD modes of the temperature in the 2D vehicle model.

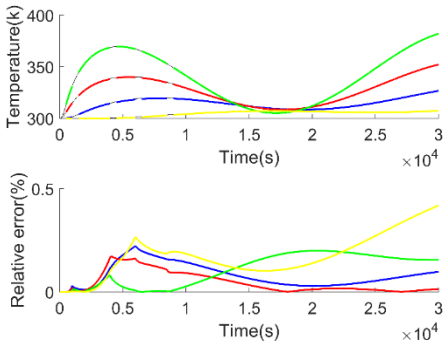

Figure 8. FOM/ROM alternation: (a) temperature at four computational cells; and (b) relative error.

In the transient analysis, 3,000 time steps are simulated assuming an initial temperature of 300 K, and then the temperature at the engine wall follows a cosine distribution in time, i.e., $T_{wall} = 300 + 50 \times \cos(2\pi t/30000)$ to evaluate ROM performance for time-varying dynamics. The simulation uses more intervals, i.e., 60 intervals and 50 time steps/interval to investigate the effects of the interval length on ROM performance. The time step and tolerance parameters remain the same.

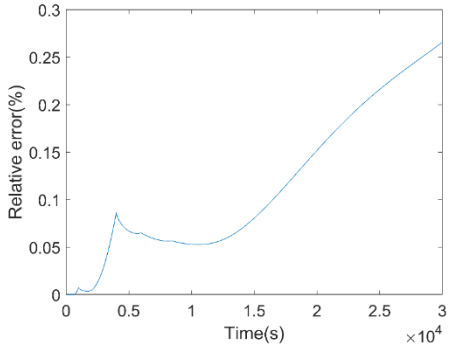

Figure 9. Relative error averaged across the entire computational domain.

In Figure 8, the temperature histories of the four computational cells same as the above are illustrated for comparison. During all the FOM intervals, although the relative errors are reduced, they cannot be brought to zero. This is because the deviation in the simulation trajectory introduced by the ROM cannot be completely eliminated by FOM simulation. It is also found that the relative error of the four selected cells during the ROM intervals oscillates rather than increasing monotonically as above. In addition, when the interval length is shorter, the FOM can respond more rapidly to correct the trajectory and reduce the error. In this case study, the FOM is used in intervals 1, 3, 9, 13, and 18, while the ROM is used in intervals 2, 4-8, 10-12, 14-17, and 19-60, contributing to 92% of the entire simulation. It is astonishing to see that the ROM is used exclusively starting from interval 19 and all the way to the end of simulation.

Figure 9 illustrates the relative error spatially averaged across the computational cells (with numbering from 10,000 to 14,000). Although its value is almost one magnitude higher than that using the FOM-only data, the ROM still exhibits excellent performance. Throughout the simulation

the relative errors stay below 0.3%, the highest value of 0.27% occurs at the end of the simulation, and the rate of the error increase becomes milder at the end of the simulation. Figure 10a and b illustrate the temperature as a function of time for 4,000 selected computational cells where the highest temperature is present. Excellent agreement is found with the maximum absolute error < 4 K at the end of the simulation as shown in Figure 10c.

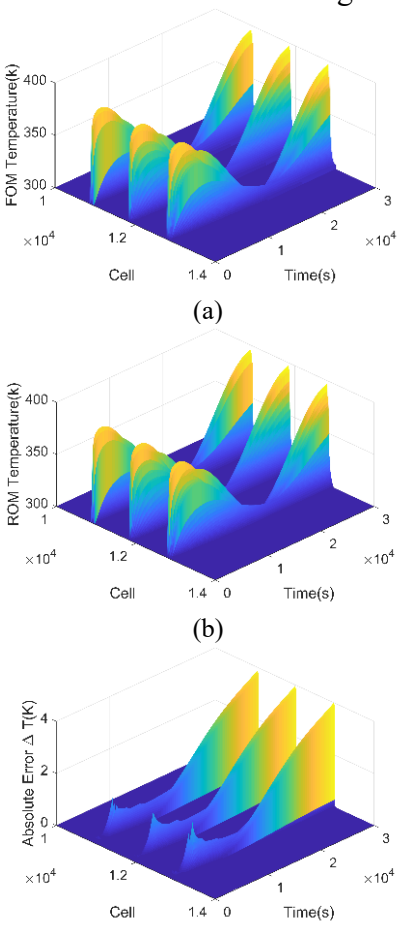

Figure 10. Comparison between (a) FOM and (b) hybrid FOM/ROM simulation in the spatiotemporal domain; and (c) absolute error

The computational efficiency of the hybrid simulation relative to a general-purpose CFD tool, CFD-ACE+ is also investigated. The FOM simulation using CFD-ACE+ takes around 1.17 seconds per time step, our customized FOM solver takes around 0.24 second per time step and ROM uses 0.025 seconds per step on the average. Thus, the speedup ratio of ROM to CFD-ACE+ in this case study is **27×**. The speedup is contributed by many ROM intervals used in the simulation and the use of our customized thermal FOM solver that is also faster than CFD-ACE+.

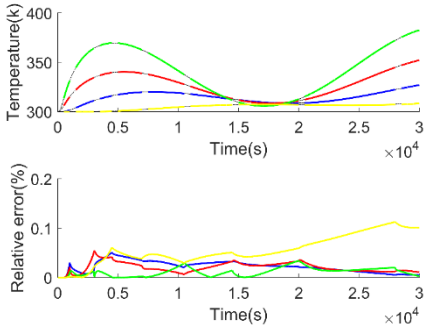

Figure 11. FOM/ROM alternation: (a) temperature at four computational cells; and (b) relative error.

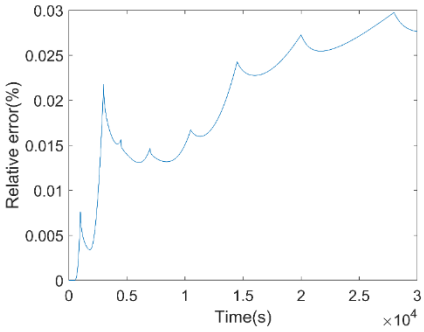

Figure 12. Relative error averaged across the entire computational domain.

There are several ways to further improve the ROM accuracy. One is to increase the energy threshold to keep more POD modes $\mathbf{U}_q$ for model switch. For example, in the results below, the energy threshold is further decreased from 1×10^{-9} to 1×10^{-10}, which signifies that the higher-order modes contributing the data representation less than 1×10^{-10} will be eliminated. Figure 11 illustrates the temperature histories of the same four computational cells within the computational domain. It clearly shows that 9 FOM intervals and 51 ROM intervals are used, which leads to the significant drop in the relative errors (below 0.1%).

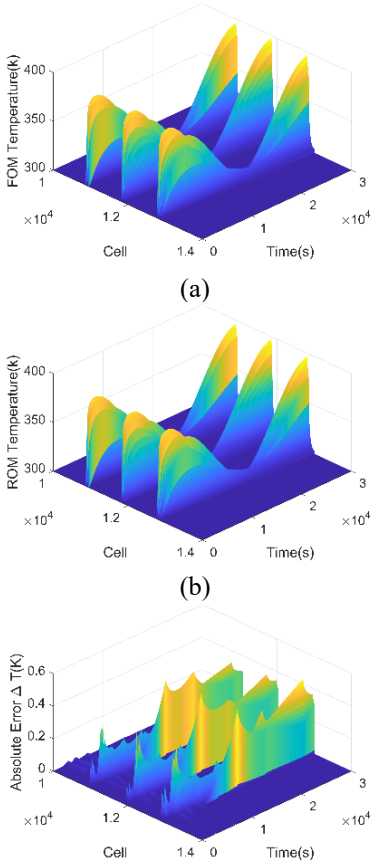

Figure 13. Comparison between (a) FOM and (b) hybrid FOM/ROM simulation in the spatiotemporal domain; and (c) absolute error

The salient performance is also manifested by Figure 12 that depicts the average relative error among computational cell numbered from 10,000 to 14,000 in the domain. The hybrid simulation demonstrates better performance than the previous case study, and the relative errors remains below 0.03% through the entire simulation. Figure 13a-b illustrate the temperature for the 4,000 selected computational cells where the highest temperature is present. Excellent agreement between them is found with the maximum absolute error less than 0.6 K as shown in Figure 13c. Given the ratio of the FOM and ROM intervals, the speedup ratio of this case study to CFD-ACE+ is 20.4×.

3.2. 3D Vehicle Mock-up

Next, we extend the hybrid simulation capability to a more computationally demanding case of a 3D vehicle model. Figure 14 illustrates the computational geometry and model. The width of the vehicle is 2.1 m, and the engine box has a width of 0.5 m. The width of the entire flow domain is 6.1 m. Similar to the cases above a temperature of 400 K following the time-dependent cosine function is set at the boundaries of the engine box. The computational domains are meshed by the hexahedral grids, yielding 989,275 computational cells (close to 1 million).

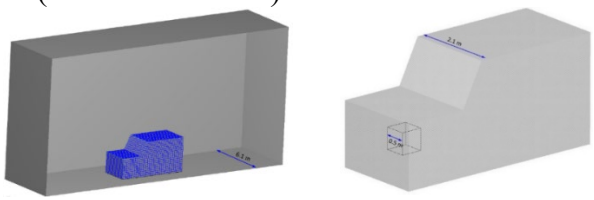

Figure 14. Computational domain and the 3D vehicle mock-up

Figure 15 depicts the spatial distribution of POD modes 1, 3, 6, and 8 of the 3D vehicle model. Similarly, the lower-order modes capture the main thermal structures at the large scale. The higher-order modes resolve the local features of the temperature distribution to enhance the model prediction through local modification.

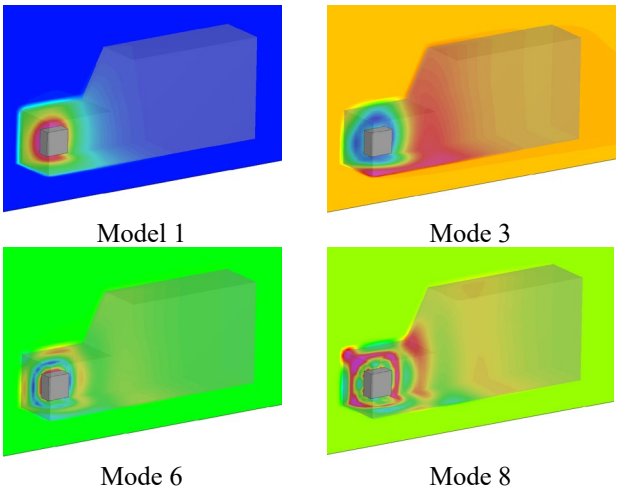

Figure 15. POD modes of the temperature in the 3D vehicle model.

In the next case study, we combine the FOM and the ROM solver together into a single framework, i.e., coupled FOM/ROM solver. 3,000 time steps are simulated, and then the temperature at the engine wall follows a cosine distribution in time. The simulation is divided into 60 intervals, and the size of the time step is dt = 10 s.

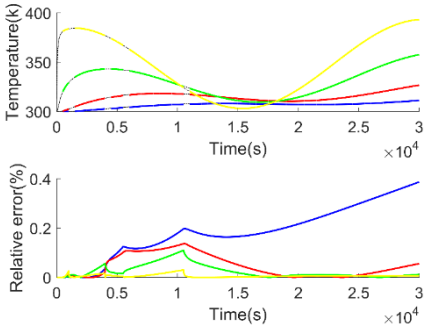

Figure 16. FOM/ROM alternation: (a) temperature at four computational cells; and (b) relative error.

Figure 16 illustrates the temperature histories of four selected computational cells. 5 out of 60 intervals are simulated using FOM, leading to utilization of ROM during 92% of the hybrid simulation. Specifically, the FOM is used in intervals 1, 3, 9, 12, and 22 only. It also clearly shows the error varies during the entire hybrid simulation, and every time the simulation switches to the FOM the error is lowered appreciably.

Figure 17 portrays the spatially averaged error of the entire computational domain. It agrees with the observation above that FOM intervals can correct the simulation trajectory and further bring down the small deviation caused by the ROM simulation. During the entire simulation the relative error stays below 0.35%.

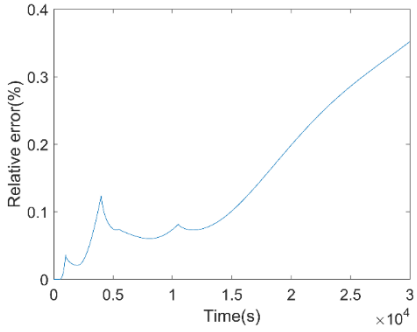

Figure 17. Relative error averaged across the entire computational domain.

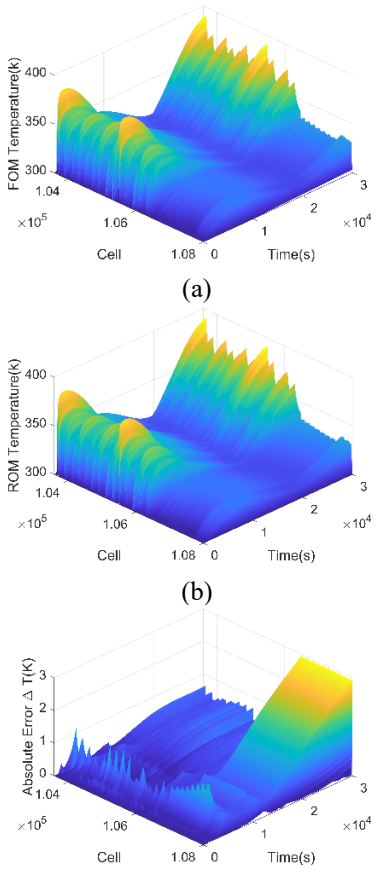

Figure 18. Comparison between (a) FOM and (b) hybrid FOM/ROM simulation in the spatiotemporal domain; and (c) absolute error

Figure 18a and b show the time-dependent results of the FOM and ROM at ~4,000 cells within the region of the highest temperature. Again, the FOM and ROM show an excellent match with the maximum absolute error ~3 K (Figure 18c). In terms of computational efficiency, the FOM simulation using CFD-ACE+ takes around 21.0185 seconds per time step. Our customized FOM and ROM solver, respectively, require 13.5 seconds and 2.5 seconds per step on the average. The interval ratio of the customized FOM to the ROM is 5:55, which leads to an effective speedup ratio of 6.2× relative to CFD-ACE+ simulation. Therefore, the use of short intervals and our FOM and ROM solver will markedly improve the computational efficiency.

4. CONCLUSION

A hybrid simulation methodology combining the CFD full order model (FOM) and the mathematically rigorous reduced order model (ROM) is developed. The simulation alternates between the FOM and the ROM to achieve salient computational performance without appreciably compromising the accuracy. The key technology components in our hybrid simulation framework including: formulation and acquisition of FOMs, POD and iPOD, ROM construction, and online model switch decision maker are all examined.

CFD simulation including both the turbulence modeling (k-ε) and thermal equation are implemented. Both models are discretized using the finite volume method and simulated to assess flow and temperature with turbulence to capture the conjugate heat transfer effect for the vehicle signature generation.

The FOM of the heat transfer is then reduced through mathematically formal MOR techniques. First, the POD technique is developed to extract the basis vectors from the FOM data, onto which the FOM can be projected yielding small models that can be solved rapidly. An iSVD method is also introduced, which is based on the "divide-and-conquer" strategy and computes the POD modes/basis vectors through low-rank SVD and basis rotation, and hence, is well-suited for our hybrid simulation and more computationally efficient. POD or iPOD are performed at the end of the FOM interval. To enable seamless alternation between the FOM and ROM, a model switch decision maker is proposed, which includes two criteria, C_{F2R} and C_{R2F}, based on the dominance of POD modes and ROM trajectory.

Case studies using two simplified 2D and 3D vehicle models that involve turbulence and conjugate heat transfer were undertaken to verify and demonstrate the proposed hybrid vehicle signature generation method. Different simulation scenarios are investigated to inspect the proposed hybrid CFD-ROM method. The hybrid simulation is extremely accurate. In all simulations, the relative error stays below 0.35% and the absolute error is <4 K. Our simulation shows that although both errors in general increase with the time at the beginning of the simulation, they will saturate as the simulation continues and be bounded.

Our hybrid simulation also demonstrates salient computational efficiency and speedup over the general-purpose CFD tool, which can be attributed to: (1) The FOM developed in this work is customized for vehicle thermal analysis, and runs faster than the general-purpose CFD solver that incurs additional computational loads; and (2) the ROM has a much smaller model order (typically 7-12), enabling significant computational acceleration. Computational acceleration > 20X is observed without need for any hardware acceleration technique. The factor that renders the speedup ratio disproportional to the model size and limits further speedup is the appreciable computational cost associated with model assembly, which will be addressed in future work.

ACKNOWLEDGEMENT

This research was sponsored by the US Army DEVCOM Ground Vehicle Systems Center (GVSC) under the contract number W56HZV-20-0086.

REFERENCES

1. Qian, J., et al., *Projection-based reduced-order modeling for spacecraft thermal analysis.* Journal of Spacecraft and Rockets, 2015. **52**(3): p. 978-989.
2. Ma, H., et al., *A Combined Data-driven and Physics-driven Method for Steady Heat Conduction Prediction using Deep Convolutional Neural Networks.* arXiv preprint arXiv:2005.08119, 2020.
3. Bai, F. and Y. Wang, *Reduced-Order Modeling Based on Hybrid Snapshot Simulation.* International Journal of Computational Methods, 2021. **18**(01): p. 2050029.
4. Bai, F. and Y. Wang, *DEIM reduced order model constructed by hybrid snapshot simulation.* SN Applied Sciences, 2020. **2**(12): p. 1-25.
5. Manhart, M. and H. Wengle, *A spatiotemporal decomposition of a fully inhomogeneous turbulent flow field.* Theoretical and computational fluid dynamics, 1993. **5**(4-5): p. 223-242.

6. Aling, H., et al. *Nonlinear Model Reduction with Application to Rapid Thermal Processing*. in *35th Conference on Decision and Control*. 1996. Kobe, Japan.
7. Białecki, R., A. Kassab, and A. Fic, *Proper orthogonal decomposition and modal analysis for acceleration of transient FEM thermal analysis.* International journal for numerical methods in engineering, 2005. **62**(6): p. 774-797.
8. Wang, Y., et al., *Model Order Reduction*, in *Encyclopedia of microfluidics and nanofluidics*, D. Li, Editor. 2008, Springer: New York. p. 1382-1391.
9. Brand, M., *Incremental singular value decomposition of uncertain data with missing values*, in *Computer Vision ECCV 2002*. 2002, Springer. p. 707-720.